Active Vibration Control of a Quarter-Car Model via a Time-delayed Vibration Absorber

Yixia Sun

School of Mechanical and Automotive Engineering, Shanghai University of Engineering Science, Shanghai 201620, China. E-mail: sunyixia@sues.edu.cn

(Received 12 July 2023; accepted 9 October 2023)

A time-delayed vibration absorber (TDVA) is proposed to suppress the vertical vibration of a quarter-car model. First, the mechanical model of the combined system with a linear TDVA is studied. Second, the vibration suppression effect of the linear TDVA at a fixed excitation frequency is experimentally verified when the passive absorber totally loses efficacy. Third, based on the system acceleration response amplitude derived by the harmonic balance method, the control parameters optimization of the nonlinear TDVA is carried out in a wide frequency band; the numerical simulation of original vibration equations is conducted to determine the stability of the system. It is concluded that the broadband vibration suppression effect of the nonlinear TDVA is obtained with optimal control parameters. The numerical results validate the correctness of the theoretical ones.

1. INTRODUCTION

Along with social progress and rapid development of the economy, vibration control of a vehicle is becoming a hot research topic. Various passive, semi-active and active control strategies are explored to improve driving comfort, handling stability and road holding of the vehicle.[1,2] Among them, passive control strategies have been widely used with the advantages of simplicity, low cost and zero energy consumption.[3] As far as active control of the vehicle, an actuation system is usually equipped to generate the desired force and an ideal control effect can be achieved in a wide frequency range.4-6 Semi-active strategies are regarded as compromises between passive and active ones, which may reduce the energy consumption while achieving acceptable vibration control effect.[7–9] In the past , with the development of computer technology, control theory and advanced material, a great deal of effort has been devoted to the study of active and semi-active vehicle vibration reduction technologies, and fruitful achievements have been made.

It is noted that time delay is inherent in active control. It derives from the process of signal acquisition and transmission, mathematical calculation and actuation.[10] At first, time delay is regarded as an adverse factor since it may weaken control effect, trigger bifurcations and chaos, and destabilize the system. Delay compensation methods are proposed to eliminate the effect of time delay.[11–13] With the intensive study of time delay problems, researchers have found that time delay is not necessarily negative. Proper time delay is effective in controlling the self-excited vibration, suppressing chaos movement, and reducing nonlinear resonant response, etc.[14–16] Therefore, time delay is intentionally introduced into an active control loop to enhance the vibration control effect and the concept of time-delayed feedback control (TDFC) emerges. Sun et al. proposed a design methodology of variable time delay in TDFC for a nonlinear isolation system.[17] Taffo et al. investigated a 2-DOFs nonlinear quarter-car model with TDFC and provided a theoretical guidance for the design of vehicles with significant vibration reduction.[18] Yan et al. designed an optimal TDFC to improve the performance of a vehicle suspension system.[19] Taffo et al. focused on the effect of TDFC on the dynamic behavior of a quarter-car model under parametric excitation, and conditions for onset of chaos resulting from heteroclinic bifurcation was derived.[20] Wang et al. studied the influence of time delay and feedback gain of TDFC on the performance of an inerter-based suspension under harmonic, random and shock excitations.[21] Liu et al. completed a theoretical and experimental study of TDFC using a flexible plate as the research object.[22]

As a well-known application of TDFC, time-delayed vibration absorbers (TDVAs) have attracted considerable attention in the field of active vibration control. The core idea of TDVAs is the introduction of an actuator via time-delayed state feedback. Wang et al. explored the effects of TDVA on the dynamic characteristics of a nonlinear multiple-layer metastructure.[23] The research results show that a single TDVA and multiple TDVAs are effective in the anti-resonance range and within a broad frequency band, respectively. Olgac et al. proposed the concept of a delayed resonator (DR).[24] With a DR attached, the vibration of the primary system can be entirely suppressed at a given frequency. The research group of Olgac further carried out a series of extensions to the classical DR, and designed dual frequency fixed DR(DFFDR), multiple-frequency DR (MFDR) and distributed DR (DDR).[25–27] Huan et al. investigated a multi-objective optimal design of a TDVA for a stochastically excited linear structure.[28] Mohanty et al. studied the nonlinear dynamics of a TDVA using a lead zirconate titanate (PZT) stack actuator and gave a clear idea as to the response amplitude of the system and the operating frequency band to minimize system vibration.[29] Yan et al. presented a general and effective time-delay control parameter optimization solving method to improve the vibration reduction effect of a nonlinear TDVA.[30]

In this paper, the linear and the nonlinear TDVAs are separately integrated into a quarter-car model. Both the inherent and the intentional time delays are taken into account in the model of the TDVA. The main research objectives are twofold. The first is to complete the experimental study to verify that the linear TDVA is effective in suppressing the vertical vibration of the quarter-car model. The second is to optimize the control parameters to improve the vibration suppression effect

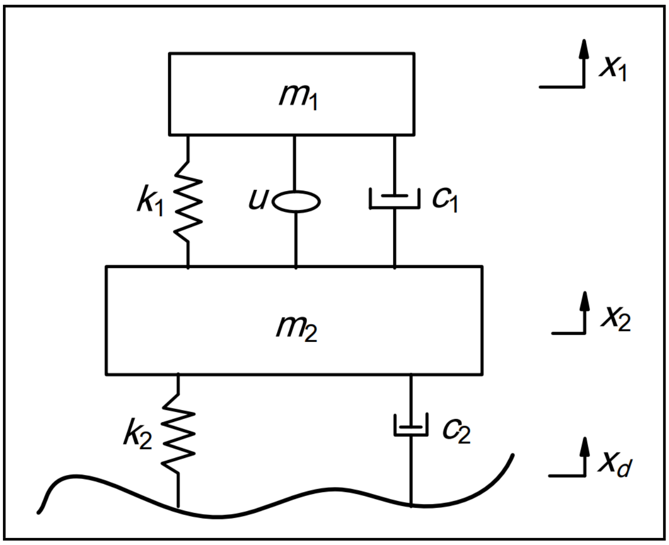

Figure 1. Quarter-car model with a linear TDVA.

of the nonlinear TDVA in a wide frequency range.

The present paper is organized as follows. In Section 2, the mechanical model of a quarter-car attached with a linear TDVA is established and experiments are carried out to illustrate the effectiveness of the linear TDVA when the passive absorber fails completely. In Section 3, the optimization of time delay and feedback gain coefficient is discussed to enhance the broadband vibration suppression effect of the nonlinear TDVA. In Section 4, conclusions are drawn and extensions are made.

2. MODEL OF A QUARTER-CAR WITH A LINEAR TDVA

2.1. Mechanical Model

Considering that vertical vibration of the vehicle body is the main factor affecting the ride comfort of the vehicle and neglecting the pitch and the roll motion of the vehicle body, the quarter-car model with a linear TDVA attached is presented in Fig. 1.[31] The absorber mass is represented in m_1 and m_2, and the vehicle body mass, respectively. The stiffness and damping coefficient of the linear TDVA are k_1 and c_1. . The suspension stiffness and damping coefficient are k_2 and c_2. The displacement of the absorber mass and the body mass are x_1 and x_2, respectively. The road displacement excitation is x_d and described by a simple harmonic function $x_d = x_0 \sin(\omega t)$. The time-delayed feedback control force is $u = g\ddot{x_1}(t-\tau)$. The feedback gain coefficient is g. The τ is the sum of the inherent time delay τ_1 and the intentional time delay τ_2. The value of τ_1 is unknown and needs to be identified for the designed feedback control loop. The value of τ_2 can be changed in the controller. The g and τ_2 are regarded as the control parameters of the linear TDVA. When $g = 0$ kg, the linear TDVA degrades into a passive vibration absorber.

According to Newton's second law, the dynamical equations of the combined system are:

$$m_1\ddot{x_1} + k_1(x_1 - x_2) + c_1(\dot{x_1} - \dot{x_2}) + g\ddot{x_1}(t-\tau) = 0; \quad (1)$$

$$m_2\ddot{x_2} + k_2(x_2 - x_d) + c_2(\dot{x_2} - \dot{x_d}) + k_1(\dot{x_2} - \dot{x_1}) - g\ddot{x_1}(t-\tau) = 0. \quad (2)$$

The solutions of Eqs. (1) - (2) are supposed to be:

$$x_1 = a_1 \sin(\omega t) + b_1 \cos(\omega t); \quad (3)$$

$$x_2 = a_2 \sin(\omega t) + b_2 \cos(\omega t). \quad (4)$$

By substituting Eqs. (3) - (4) into Eqs. (1) - (2) and extracting the coefficients of and from both sides of the equations, one has:

$$\{a_1, b_1, a_2, b_2,\}^T = D^{-1}F; \quad (5)$$

in which D and F are given by Eqs. (6) and (7), respectively - see the top of the next page.

Then, the acceleration amplitudes G_1 and G_2 of the absorber and the body are calculated to be:

$$G_1 = \omega^2\sqrt{a_1^2 + b_1^2}; \quad (8)$$

$$G_2 = \omega^2\sqrt{a_2^2 + b_2^2}. \quad (9)$$

2.2. Experiments

2.2.1. Experimental setup

The photo of the experimental structure is shown in Fig. 2. A primary mass 2 is supported on a fixed base 1 by two primary springs 9. A servo motor 3 is fixed on the primary mass. An absorber mass 5 is connected to the primary mass by two secondary springs 7. A cover plate 6 is connected to the base by four guide bars 13. Two linear bearings 4 are installed on the absorber mass to ensure that the primary mass and the absorber mass vibrate only in the vertical direction. The upper and the lower ends of the tension spring 11 are respectively linked to the hook 10 and the motor shaft sleeve 8 by a steel wire rope 12. The schematic of the TDFC experiment is illustrated in Fig. 3. The experimental system consists of three parts: excitation, signal acquisition and processing, and actuation.

Excitation: As shown in Fig. 4, the base of the experimental structure is fixed on a vibration table, which vibrates vertically under the drive of an amplifier. The vibration form is set as simple harmonic vibration with adjustable frequency and amplitude.

Signal acquisition and processing: Three acceleration sensors are used to measure the acceleration signals of the base, primary mass and absorber mass, respectively. The three acceleration signals then enter the VR9500 signal acquisition instrument, where the acceleration data are recorded and then enter the signal conditioning instrument. In the signal conditioning instrument, the functions of low-pass filtering, signal amplification and voltage lifting are implemented to improve the signal-to-noise ratio.

Actuation: First, the processed signal goes into Euro404 motion controller, which communicates with a computer. The time-delayed feedback control instruction is written in Euro404 motion controller and then transferred to the servo controller. Second, the shaft of the servo motor rotates under the drive of the servo controller. Third, the low end of the tension spring moves vertically as a consequence of the rotation of the motor shaft and applies the control force.

$$D = \begin{bmatrix} k_1 - m_1\omega^2\cos(\omega\tau) & -c_1\omega^2 - g\omega^2\sin(\omega\tau) & -k_1 & c_1\omega \\ c_1\omega^2 + g\omega^2\sin(\omega\tau) & k_1 - m_1\omega^2\cos(\omega t) & -c_1\omega & -k_1 \\ -k_1 + g\omega^2\cos(\omega\tau) & c_1\omega + g\omega^2\sin(\omega\tau) & k_1 + k_2 - m_2\omega^2 & -c_1\omega - c_2\omega \\ -c_1\omega - g\omega^2\sin(\omega\tau) & -k_1 + g\omega^2\cos(\omega\tau) & c_1\omega + c_2\omega & k_1 + k_2 - m_2\omega^2 \end{bmatrix}; \tag{6}$$

$$F = [0, 0, k_2, x_0, c_2x_0\omega]^T. \tag{7}$$

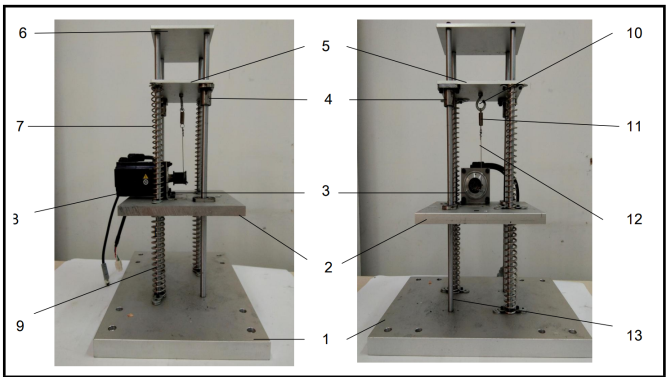

Figure 2. Photo of the experimental structure, (1 base, 2 primary mass, 3 servo motor, 4 linear bearing, 5 absorber mass, 6 cover plate, 7 secondary spring, 8 motor shaft sleeve, 9 primary spring, 10 hook, 11 tension spring, 12 steel wire rope, 13 guide bar).

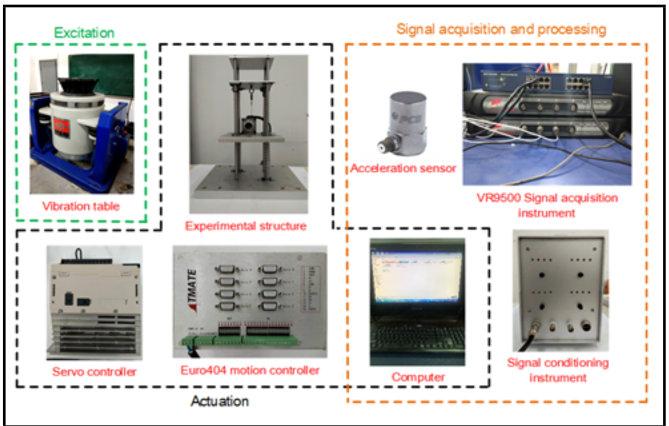

Figure 3. Schematic of TDFC experiment.

2.2.2. Physical parameters identification

As a premise, the physical parameters values of the combined system need to be identified. Letting $x_d = 0$ m and applying a sinusoidal excitation force $f\sin(\omega t)$ to the primary mass, the dynamical equations of the system without TDFC are:

$$m_1\ddot{x}_1 + k_1(x_1 - x_2) + c_1(\dot{x}_1 - \dot{x}_2) = 0; \tag{10}$$

$$m_2\ddot{x}_2 + k_2x_2 + c_2\dot{x}_2 + k_1(x_2 - x_1) + c_1(\dot{x}_2 - \dot{x}_1) = 0. \tag{11}$$

The solutions of Eqs. (10) - (11) are assumed to be:

$$x_1 = X_1e^{j\omega t}; x_2 = X_2e^{j\omega t}; \tag{12}$$

where X_1 and X_2 are complex.

Substituting Eq. (12) into Eqs. (10) and (11) gives:

$$\begin{bmatrix} X_1 \\ X_2 \end{bmatrix} = \frac{f}{\Delta(\omega)}\begin{bmatrix} k_1 + jc_1\omega \\ k_1 - m_1\omega^2 + jc_1\omega \end{bmatrix}; \tag{13}$$

in which $\Delta(\omega) = (k_1 - m_1\omega^2 + jc_1\omega)(k_1Kk_2 - m_2\omega^2 + jc_1\omega + jc_2\omega) - (k_1 + jc_1\omega)^2$.

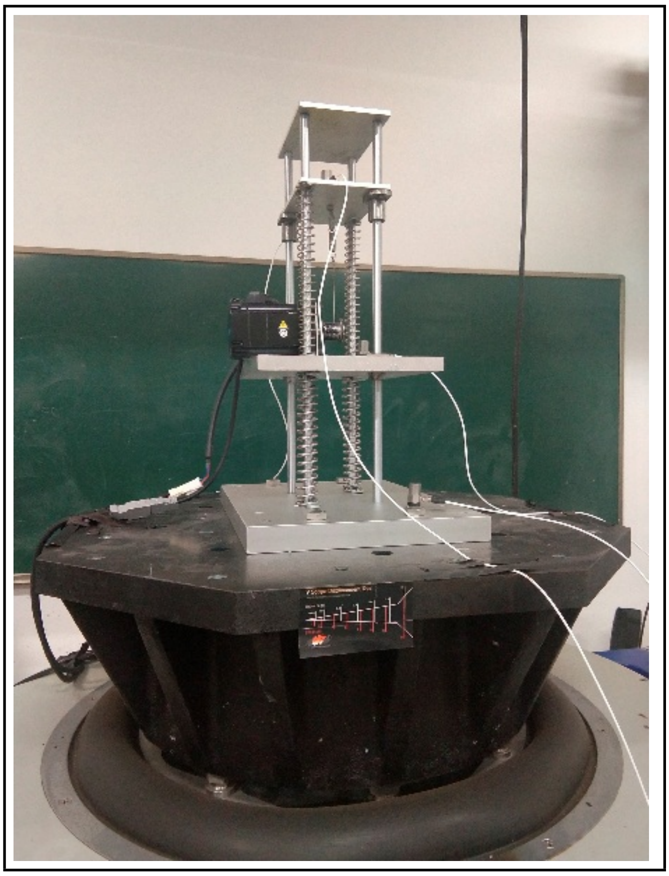

Figure 4. Installation of the experiment structure.

Table 1. Physical parameters of the system.

Parameter	Value	Parameter	Value	Parameter	Value
m_1 (kg)	0.3	k_1 (Nm^{-1})	2229.77	c_1 (Nsm^{-1})	2.29
m_2 (kg)	3.5	k_2 (Nm^{-1})	9366.75	c_2 (Nsm^{-1})	45.22

We define H_1 and H_2 to be the acceleration transfer functions of the absorber and the primary system, namely, the ratio of the amplitude of the acceleration response and that of the excitation force. Hence, the theoretical expressions of H_1 and H_2 are:

$$H_1 = \frac{\omega^2|X_1|}{f}; \frac{\omega^2|X_2|}{f}. \tag{14}$$

Applying a hammer excitation to the primary mass, the acceleration transfer function-frequency curves of the system are recorded. Based on Eq. (14) and the least-squares method, the values of the physical parameters are identified and listed in Table 1. Fig. 5 shows the comparison of the experimental and the theoretical results of the acceleration transfer function-frequency curves, where $\Omega = \omega/(2\pi)$ denotes the frequency of the excitation force.

According to the stability analysis in reference,[23] the stability zoning diagram of the system is shown in Fig. 6. The system is stable when the values of g and τ locate in region I,

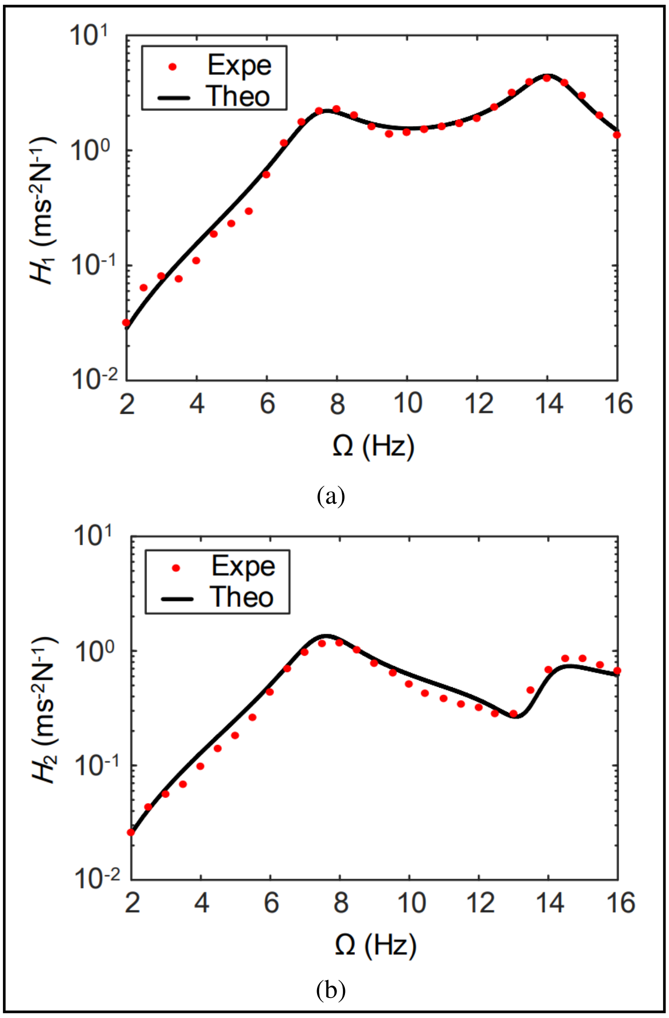

Figure 5. Acceleration transfer function-frequency curves of the system without TDFC: (a) absorber and (b) primary system, red dots are experimental results; black line is theoretical result.

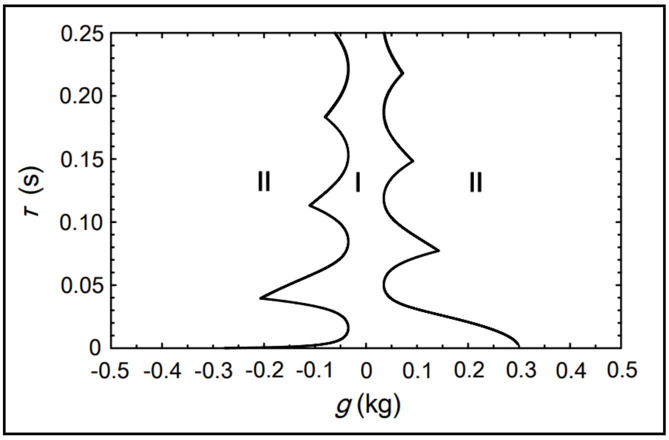

Figure 6. Stability zoning diagram.

while unstable when the values of g and τ locate in region II.

2.2.3. Identification of inherent time delay

The identification process of the inherent time delay τ_1 existing in the designed feedback control loop is as follows.

First, a hammer excitation is applied to the primary mass and an acceleration sensor is used to monitor the response of the absorber mass.

Second, the acceleration signal of the absorber mass is divided into two branches. One branch enters channel 1 of the signal acquisition instrument. The other branch goes successively into the signal conditioning instrument and Euro404 motion controller. In Euro404 motion controller, a feedback control command without the intentional time delay is written and then transmitted into the servo controller.

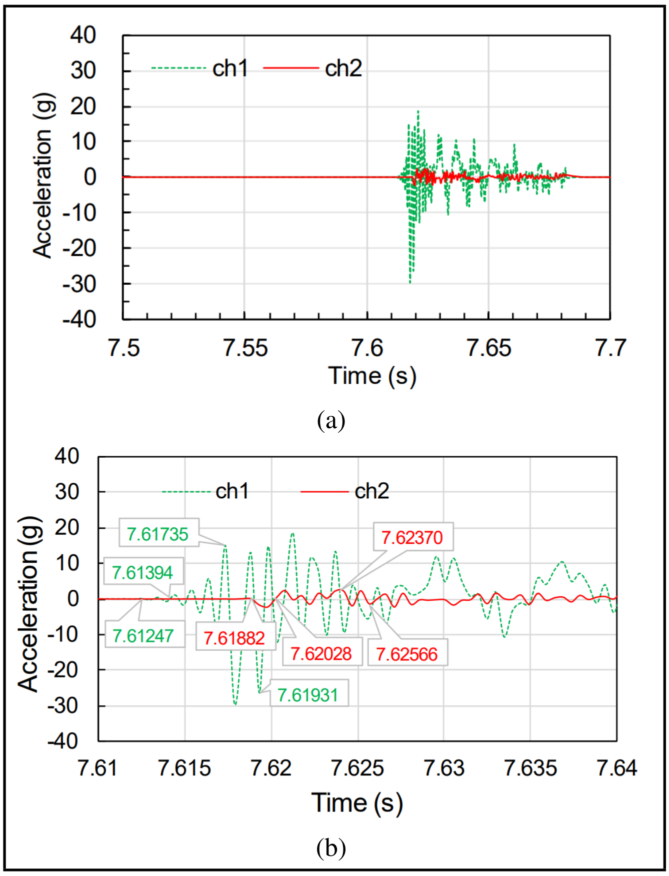

Figure 7. Acceleration signals of channels 1 and 2:(a) partial time history, (b) zoom of (a).

Third, the shaft of the servo motor begins to rotate under the drive of the servo controller. The tangential acceleration signal of the servo motor shaft is measured by a three-phase acceleration sensor and then transmitted into channel 2 of the signal acquisition instrument.

As thus, τ_1 is considered as the time lag between the signals of channels 1 and 2. Fig. 7 (a) shows the acceleration signals of channels 1 and 2. Fig. 7 (b) is zoom of Fig. 7 (a). The time points when the peaks, troughs, zero-crossings and initial signal values of channels 1 and 2 occur are shown in Fig. 7 (b) and Table 2. The value of τ_1 is calculated to be 6.35 ms. The experiment is repeated twice and the values of τ_1 are identified to be 6.34 ms and 6.35 ms, respectively. The average value of τ_1 is 6.35 ms.

2.2.4. Experimental study of the vibration suppression effect

From Fig. 5, the two resonant frequencies of the combined system are approximately 8 Hz and 14 Hz. The anti-resonant frequency of the combined system is 13.5 Hz, which closes to the second resonant frequency. It means that the passive vibration absorber is fully effective for $\Omega = 13.5$ Hz, while it fails completely for $\Omega = 8$ Hz and 14 Hz. Whether the TDVA could bring a better vibration suppression effect for $\Omega = 8$ Hz is our major concern here.

Table 2. Identification of τ_1.

	peak		trough		zero-crossing		initial signal value	
	chl	ch2	chl	ch2	chl	ch2	chl	ch2
time points (s)	7.61735	7.62370	7.61931	7.62566	7.61394	7.62028	7.61247	7.61882
time lag (ms)	6.35		6.35		6.34		6.35	

Fig. 8 shows the measured displacement amplitude x_0 of the base excitation and the corresponding system acceleration amplitudes G_1 and G_2 for $\Omega = 8$ Hz. The total sampling time is 2.5 minutes. For $0 \leq t < 1$ min, the TDFC is deactivated, that is, $g = 0$ kg. For 1 min$\leq t \leq 2.5$ min, the TDFC with $g = 0.14$ kg and $\tau = 0.026$ s is activated. From Fig. 8 (a), the displacement amplitude of the base excitation remains at 0.25 mm after an initial transient. From Figs. 8 (b) and 8 (c), G_1 reduces from 3.70 ms^{-2} to 3.41 ms^{-2} and G_2 reduces from 2.47 $^{-2}$ to 2.25 $^{-2}$. It is noted that the introduction of the TDFC improves the vibration suppression effect of the absorber. The theoretical result of G_1 given by Eq. (8) is 3.86 $^{-2}$ for $g = 0$ kg and 3.53 $^{-2}$ for $g = 0.14$ kg, $\tau = 0.026$ s. The theoretical result of G_2 given by Eq. (9) is 2.55 $^{-2}$ for $g = 0$ kg and 2.30 $^{-2}$ for $g = 0.14$ kg, $\tau = 0.026$ s. Therefore, the experimental results agree with the theoretical ones. Fig. 9 shows the numerical simulation of system acceleration responses for $x_0 = 0.25$ mm and $\Omega = 8$ Hz. It should be pointed out that that the TDVA with $g = 0.14$ kg and $\tau = 0.026$ s does not significantly improve the vibration suppression effect. Hence, the optimization of the control parameters will be considered to maximize the vibration suppression effect of TDVA in Section 3.

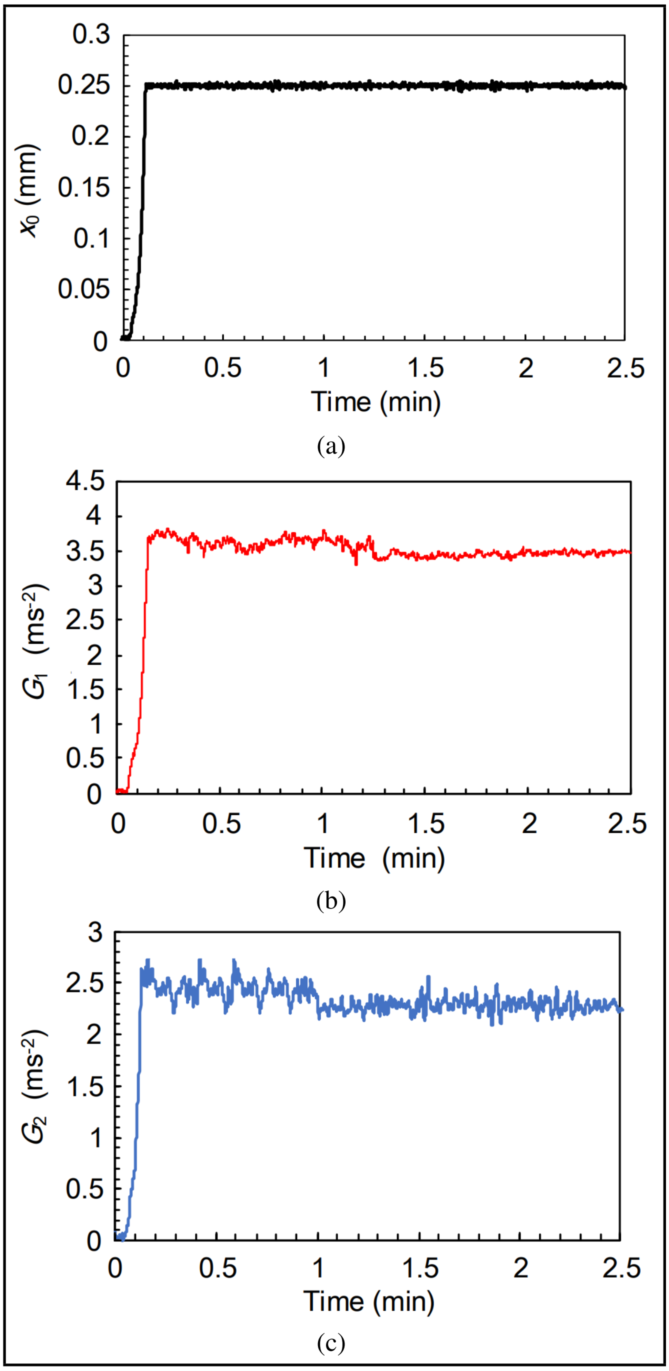

Figure 8. Measured excitation and response acceleration amplitudes: (a) base, (b) absorber and (c) primary system.

3. PARAMETER OPTIMIZATION OF THE NONLINEAR TDVA

3.1. Modelling

Previous studies have shown that the vibration control effect may be enhanced and the frequency band of vibration reduction may be broadened by properly introducing the nonlinear elements into TDVAs. Inspired by this result, a spring with cubic nonlinearity is added into the liner TDVA and the control parameters optimization are further discussed to improve the vibration suppression effect of the nonlinear TDVA.

The dynamical equations of the nonlinear system are:

$$m_1\ddot{x_1} + c_1(\dot{x_1} - \dot{x_2}) + k_1(x_1 - x_2) + \delta(x_1 - x_2)^3 + g\ddot{x}_1(t - \tau) = 0; \quad (15)$$

$$m_2\ddot{x_2} + c_1(\dot{x_1} - \dot{x_2}) - k_1(x_1 - x_2) - \delta(x_1 - x_2)^3 + c_2(\dot{x_2} - \dot{x_d}) + k_2(x_2 - x_d) - g\ddot{x}_1(t - \tau) = 0; \quad (16)$$

where δ_1 is the nonlinear stiffness coefficient of the TDVA and the other physical parameters have the same meaning and values as before.

According to the harmonic balance method, the solutions of Eqs. (15) and (16) are written as:

$$x_1 = r_1 \sin(\omega t) + r_2 \cos(\omega t); \quad (17)$$

$$x_2 = r_3 \sin(\omega t) + r_4 \cos(\omega t). \quad (18)$$

Substituting Eqs. (17) - (18) into Eqs. (15) - (16) and collecting the like terms, we have:

$$U_1 \sin(\omega t) + V_1 \cos(\omega t) = 0; \quad (19)$$

$$U_2 \sin(\omega t) + V_2 cos(\omega t) = 0; \quad (20)$$

where the expressions of U_1, V_1, U_2 and V_2 refer to Appendix A.

Letting $U_1 = V_1 = U_2 = V_2 = 0$, the values of r_1, r_2, r_3 and r_4 can be numerically solved. The acceleration amplitude Q_1 and Q_2 of the nonlinear TDVA and the primary system are:

$$Q_1 = \omega^2\sqrt{r_1^2 + r_2^2}; \quad (21)$$

$$Q_2 = \omega^2\sqrt{r_3^2 + r_4^2}. \quad (22)$$

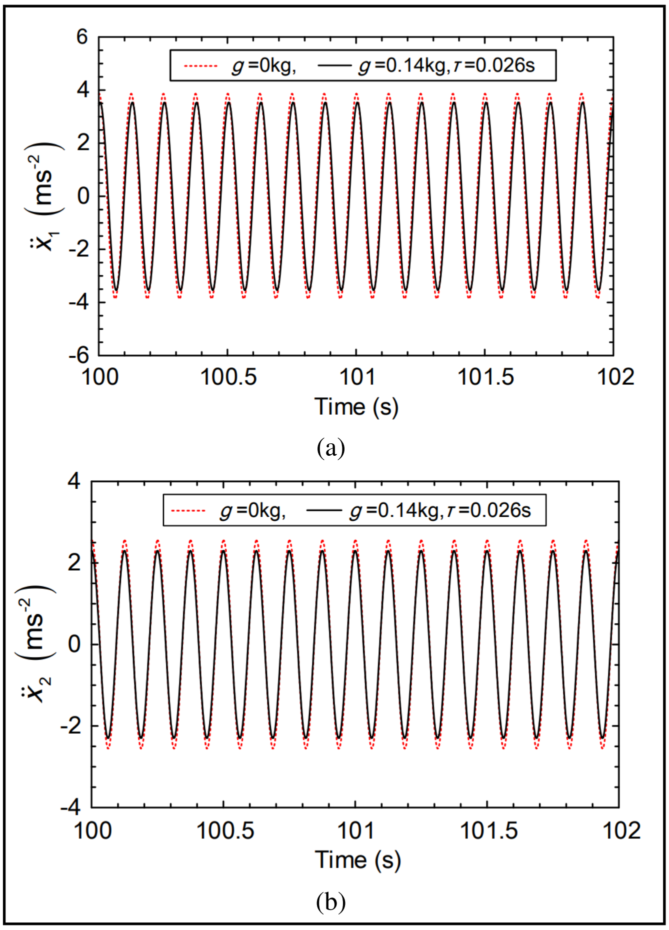

Figure 9. Numerical simulation of system acceleration responses: (a) absorber and (b) primary system.

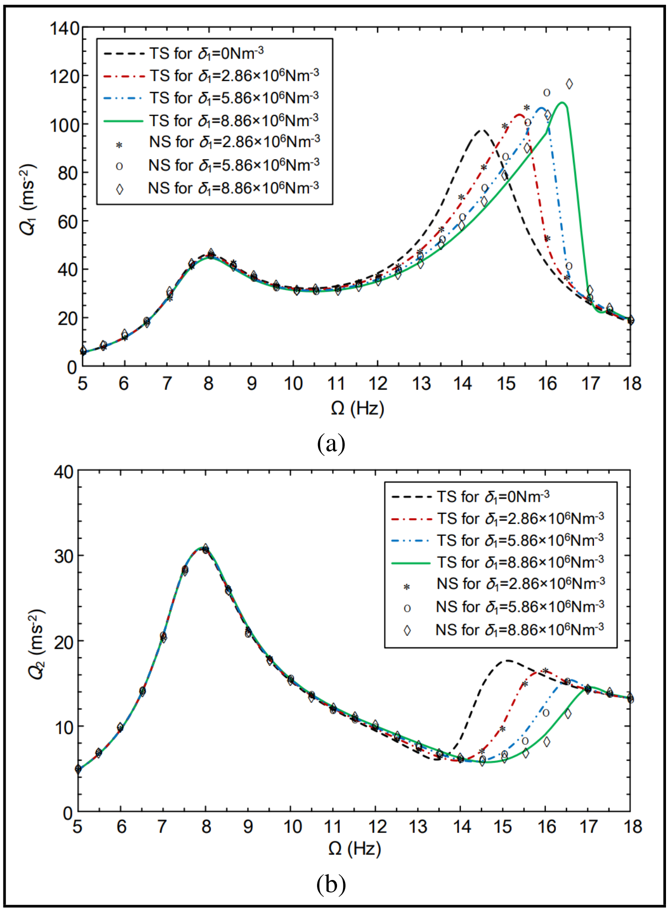

Figure 10. System acceleration amplitude-frequency curves: (a) passive nonlinear absorber and (b) primary system.

For different δ_1, Fig. 10 shows the theoretical solution (TS) and numerical solution (NS) of the system acceleration amplitude-frequency curves, where $x_0 = 0.003$ m. It is noted that the numerical solutions are in good agreement with the theoretical ones. The frequency band of vibration reduction becomes wider as increasing δ_1.

3.2. Control Parameter Optimization

To improve the vibration suppression effect of the nonlinear TDVA, the control parameter optimization is discussed in this section. The time delay τ and feedback gain coefficient g are the parameters to be optimized. Minimum primary system acceleration amplitude is the optimization objective. The optimization process is as follows.

Step 1: The value ranges of the parameters Ω, g and τ are determined as $\Omega \in [5 \text{ Hz}, 18 \text{ Hz}]$, $g \in [-0.3 \text{ kg}, 0 \text{ kg}) \cup (0 \text{ kg}, 0.3 \text{ kg}]$ and $\tau \in (0, 0.25 \text{ s}]$.

Step 2: The parameters Ω, g and τ are respectively discretized at intervals of 0.5 Hz, 0.001 kg and 0.001 s, respectively. Discrete values $\Omega_i (i = 1, 2, \cdots, 27)$, $g_k (k = 1, 2, \cdots, 600)$ and $\tau_l (l = 1, 2, \cdots, 250)$ are obtained. 1.5×10^5 sets (g_k, τ_l) of control parameters are thus recorded.

Step 3: For $\Omega = \Omega_1$, each set of control parameters are successively substituted into Eqs. (21) - (22), and values of the primary system acceleration amplitude are calculated. Among them, Minimum value Q_{2min1} is chosen and the corresponding values of control parameters are regarded as the optimal values indicated as g_{op1} and τ_{op1}.

Step 4: Numerical simulation of Eqs. (15) - (16) are carried out to verify the stability of the system. If the system is stable, Q_{2min1}, g_{op1} and τ_{op1} for $\Omega = \Omega_1$ are outputted. Otherwise, the three values are removed and the above process is repeated until the system is stable.

Step 5: By repeating Steps 3 and 4, the optimal values of control parameters for other discrete frequency points are obtained.

The optimization results for $\sigma_1 = 8.86106 \text{ Nm}^{-3}$ are shown in Appendix B. The system acceleration amplitude-frequency curves with and without the optimal control parameters are presented in Fig. 11. Clearly, for 9.5 Hz$< \Omega < 17.5$ Hz, the acceleration amplitude of the primary system significantly decreases while that of the absorber increases when the optimal parameters are introduced. Then the vibration energy is transferred from the primary system to the absorber and the vibration control effect of the absorber is improved by optimizing the control parameters. Fig. 12 illustrates the numerical simulation of system acceleration responses for $\Omega = 17$ Hz and $x_0 = 0.003$ m. From Fig. 12, the acceleration amplitude of the primary system is reduced by 50 %, while that of the absorber is increased by 196 %. The numerical result is in agreement with the corresponding theoretical result shown in Appendix B.

4. CONCLUSION AND EXTENSIONS

An active vibration control of the quarter-car model via the linear and the nonlinear TDVA is respectively presented. The conclusions and extensions are summarized as follows.

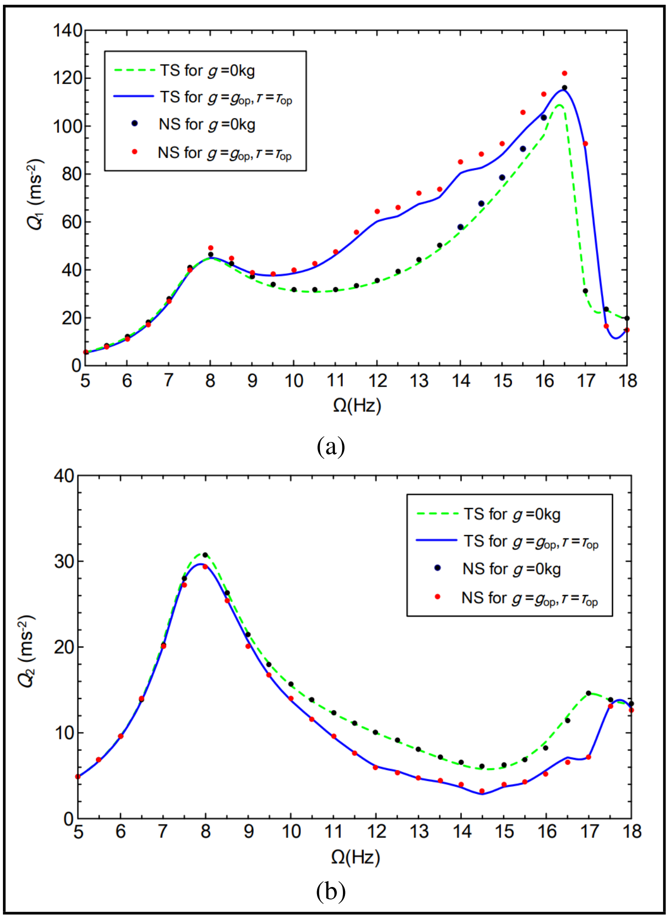

Figure 11. System acceleration amplitude-frequency curves when $\sigma_1 = 8.86106$ Nm^{-3}: (a) absorber and (b) primary system.

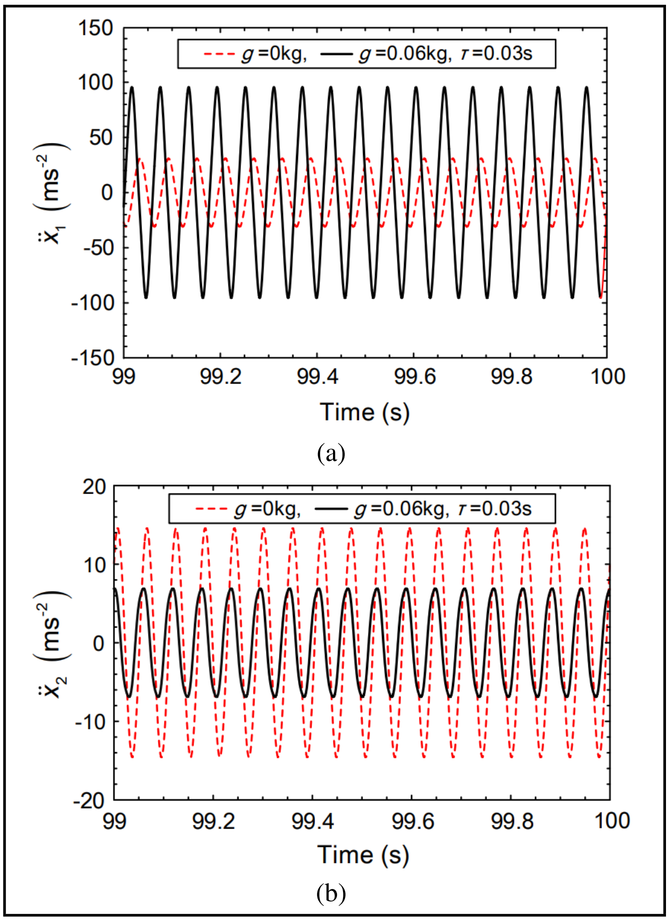

Figure 12. Numerical simulation of system acceleration responses for $\Omega = 17$ Hz and $x_0 = 0.003$ m: (a) absorber and (b) primary system.

1. The value of the inherent time delay in the designed feedback control loop was identified to be 6.35 ms by the hammer test. The linear TDVA with $g = 0.14$ kg and $\tau = 0.026$ s decreased the acceleration amplitude of the primary system by about 10 %.

2. The vibration suppression effect of the nonlinear TDVA was improved by the control parameters optimization. Especially, for $\Omega = 17$ Hz, the nonlinear TDVA with optimal control parameters decreased the acceleration amplitude of the primary system by 50 %. In addition, energy transfer between the nonlinear absorber and the primary system occurred at some excitation frequencies.

3. To maximize the vibration control effect, the control parameters of the linear TDVA were expected to be optimized. Moreover, the effectiveness of the optimized linear and nonlinear TDVA will be verified in further experiments.

ACKNOWLEDGEMENTS

This research is funded by the National Natural Science Foundation of China (No. 11602135).

REFERENCES

[1] Shen, Y. J., Chen, L., Yang, X. F., et al. Improved design of dynamic vibration absorber by using the inerter and its application in vehicle suspension, *Journal of Sound and Vibration*, **361**,148-158, (2016). https://doi.org/10.1016/j.jsv.2015.06.045

[2] Hu, Y. L., Chen, M. Z. Q. and Shu, Z. Passive vehicle suspensions employing inerters with multiple performance requirements, *Journal of Sound and Vibration*, **333**(8), 2212-2225, (2014). https://doi.org/10.1016/j.jsv.2013.12.016

[3] Fossati, G. G., Miguel, L. F. F. and Casas, W. J. P. Multi-objective optimization of the suspension system parameters of a full vehicle model, *Optimization and Engineering*, **20**(1), 151-177, (2019). https://doi.org/10.1007/s11081-018-9403-8

[4] Kumar, S., Medhavi, A., Kumar, R., et al. Modeling and analysis of active full vehicle suspension model optimized using the advanced fuzzy logic controller, *International Journal of Acoustics and Vibration*, **27**(1), 26-36, (2022). https://doi.org/10.20855/ijav.2022.27.11825

[5] Pan, H. H. and Sun, W. C. Nonlinear output feedback finite-time control for vehicle active suspension systems, *IEEE Transactions on Industrial Informatics*, **15**(4), 2073-2082, (2019). https://doi.org/10.1109/tii.2018.2866518

[6] Taskin, Y., Yuksek, I. and Yagiz, N. Vibration control of vehicles with active tuned mass damper, *Journal of Vibroengineering*, **19**(5), 3533-3541, (2017). https://doi.org/10.21595/jve.2017.18138

[7] Chen, M. Z. Q., Hu, Y. L., Li, C. Y., et al. Application of semi-active inerter in semi-active suspensions via force tracking, *Journal of Vibration and Acoustics*, **138**(4), Article ID:041014, (2016). https://doi.org/10.1115/1.4033357

8 Yoon, D. S., Kim, G. W. and Choi, S. B. Response time of magnetorheological dampers to current inputs in a semi-active suspension system: Modeling, control and sensitivity analysis, *Mechanical Systems and Signal Processing*, **146**, Article ID:106999, (2020). https://doi.org/10.1016/j.ymssp.2020.106999

9 Pozo, F., Zapateiro, M., Acho, L., et al. Experimental study of semiactive VSC techniques for vehicle vibration reduction, *Journal of the Franklin Institute-Engineering and Applied Mathematics*, **350**(1), 1-18, (2013). https://doi.org/10.1016/j.jfranklin.2012.11.008

10 Liu, K., Chen, L. X., Cai, G. P., et al. Robust H∞ control of building structures with time delay, *International Journal of Acoustics and Vibration*, **22**(1), 14-26, (2017). https://doi.org/10.20855/ijav.2017.22.1446

11 Liu, L., Zhang, S., Xue, D. Y., et al. Robust stability analysis for fractional-order systems with time delay based on finite spectrum assignment, *International Journal of Robust and Nonlinear Control*, **29**(8), 2283-2295, (2019). https://doi.org/10.1002/rnc.4490

12 Sung, S., Kang, H. J., Shim, H., et al. Compensation technique for delay times of various feedback filters in a three-phase control system for synchronous machines, *Journal of Electrical Engineering & Technology*, **16**(6), 3069-3080, (2021). https://doi.org/10.1007/s42835-021-00831-4

13 Gao, J. Q., Gong, C., Li, W. Z., et al. Novel compensation strategy for calculation delay of finite control set model predictive current control in PMSM, *IEEE Transactions on Industrial Electronics*, **67**(7), 5816-5819, (2020). https://doi.org/10.1109/tie.2019.2934060

14 Sarkar, A. Mondal, J. and Chatterjee, S. Controlling self-excited vibration using positive position feedback with time-delay, *Journal of the Brazilian Society of Mechanical Sciences and Engineering*, **42**(9), Article ID:464, (2020). https://doi.org/10.1007/s40430-020-02544-7

15 Liu, C. X., Yan, Y. and Wang, W. Q. Resonances and chaos of electrostatically actuated arch micro/nanoresonators with time delay velocity feedback, *Chaos Solitons & Fractals*, **131**, Article ID:109512, (2020). https://doi.org/10.1016/j.chaos.2019.109512

16 Peng, J., Zhang, G., Xiang, M. J., et al. Vibration control for the nonlinear resonant response of a piezoelectric elastic beam via time-delayed feedback, *Smart Materials and Structures*, **28**(9), Article ID:095010, (2019). https://doi.org/10.1088/1361-665x/ab2e3d

17 Sun, X. T., Wang, F. and Xu, J. Dynamics and realization of a feedback-controlled nonlinear isolator with variable time delay, *Journal of Vibration and Acoustics*, **141**(2), Article ID:021005, (2019). https://doi.org/10.1115/1.4041369

18 Koumene Taffo, G. I., Siewe, M. S. and Tchawoua, C. Stability switches and bifurcation in a two-degrees-of-freedom nonlinear quarter-car with small time-delayed feedback control, *Chaos Solitons & Fractals*, **87**, 226-239, (2016). https://doi.org/10.1016/j.chaos.2016.04.012

19 Yan, G., Fang, M. and Xu, J. Analysis and experiment of time-delayed optimal control for vehicle suspension system, *Journal of Sound and Vibration*, **446**, 144-158, (2019). https://doi.org/10.1016/j.jsv.2019.01.015

20 Koumene Taffo, G. I. and Siewe, M. S. Parametric resonance, stability and heteroclinic bifurcation in a nonlinear oscillator with time-delay: Application to a quarter-car model, *Mechanics Research Communications*, **52**, 1-10, (2013). https://doi.org/10.1016/j.mechrescom.2013.05.007

21 Wang, Y., Jin, X. Y., Zhang, Y. S., et al. Dynamic performance and stability analysis of an active inerter-based suspension with time-delayed acceleration feedback control, *Bulletin of the Polish Academy of Sciences-Technical*, **70**(2), Article ID: e140687, (2022). https://doi.org/10.24425/bpasts.2022.140687

22 Liu, K., Chen, L. X. and Cai, G. P. An experimental study of delayed positive feedback control for a flexible plate, *International Journal of Acoustics and Vibration*, **17**(4), 171-180, (2012). https://doi.org/10.20855/ijav.2012.17.4312

23 Wang, F., Sun, X., Meng, H., et al. Tunable broadband low-frequency band gap of multiple-layer metastructure induced by time-delayed vibration absorbers, *Nonlinear Dynamics*, **107**(3), 1903-1918, (2022). https://doi.org/10.1007/s11071-021-07065-z

24 Olgac, N. and Holm-Hansen, B. T. A novel active vibration absorption technique: delayed resonator, *Journal of Sound and Vibration*, **176**, 93-104, (1994). https://doi.org/10.1006/jsvi.1994.1360

25 Olgac, N., Elmali, H. and Vijayan, S. Introduction to the dual frequency fixed delayed resonator, *Journal of Sound and Vibration*, **189**, 355-367, (1996). https://doi.org/10.1006/jsvi.1996.0024

26 Valasek, M., Olgac, N. and Neusser, Z. Real-time tunable single-degree of freedom, multiple-frequency vibration absorber, *Mechanical Systems and Signal Processing*, **133**, Article ID:106244, (2019). https://doi.org/10.1016/j.ymssp.2019.07.025

27 Pilbauer, D., Vyhlidal, T. and Olgac, N. Delayed resonator with distributed delay in acceleration feedback-design and experimental verification, *IEEE-ASME Transactions on Mechatronics*, **21**(4), 2120-2131, (2016). https://doi.org/10.1109/tmech.2016.2516763

28 Huan, R. H., Chen, L. X. and Sun, J. Q. Multi-objective optimal design of active vibration absorber with delayed feedback, *Journal of Sound and Vibration*, **339**, 56-64, (2015). https://doi.org/10.1016/j.jsv.2014.11.019

29 Mohanty, S. and Dwivedy, S. K. Nonlinear dynamics of piezoelectric-based active nonlinear vibration absorber using time delay acceleration feedback, *Nonlinear Dynamics*, **98**(2), 1465-1490, (2019). https://doi.org/10.1007/s11071-019-05271-4

30 Yan, T., Ren, C., Zhou, J., et al. The study on vibration reduction of nonlinear time-delay dynamic absorber under external excitation, *Mathematical Problems in Engineering*, **2020**, Article ID: 8578596, (2020). https://doi.org/10.1155/2020/8578596

31 Li, Y. L., Lei, J. and Li, W. X. Semiactive control for SDOF vehicle suspension on IVNs via delayed positive feedback, *Integrated Ferroelectrics*, **160**(1), 90-105, (2015). https://doi.org/10.1080/10584587.2015.1033938

APPENDIX A

$$
\begin{aligned}
U_1 =& k_1 r_1 - m_1\omega^2 r_1 + \frac{3}{4}\delta_1 r_1^3 - c_1\omega r_2 + \frac{3}{4}\delta_1 r_1 r_2^2 - k_1 r_3 - \frac{9}{4}\delta_1 r_1^2 r_3 + \frac{3}{4}\delta_1 r_2^2 r_3 + \frac{9}{4}\delta_1 r_1 r_3^2 - \frac{3}{4}\delta_1 r_3^3 + \\
& c_1\omega r_4 - \frac{3}{2}\delta_1 r_1 r_2 r_4 + \frac{3}{2}\delta_1 r_1 r_2 r_3 r_4 + \frac{3}{4}\delta_1 r_1 r_4^2 - \frac{3}{4}\delta_1 r_3 r_4^2 - g\omega^2 r_1 \cos(\omega\tau) - g\omega^2 r_2 \sin(\omega\tau);\\
V_1 =& c_1\omega r_1 + k_1 r_2 - m_1\omega^2 r_2 + \frac{3}{4}\delta_1 r_1^2 r_2 + \frac{3}{4}\delta_1 r_2^3 - c_1\omega r_3 - \frac{3}{2}\delta_1 r_1 r_2 r_3 + \frac{3}{4}\delta_1 r_2 r_3^2 - k_1 r_4 - \frac{3}{4}\delta_1 r_1^2 r_4 - \\
& \frac{9}{4}\delta_1 r_2^2 r_4 + \frac{3}{2}\delta_1 r_1 r_3 r_4 - \frac{3}{4}\delta_1 r_3^2 r_4 + \frac{9}{4}\delta_1 r_2 r_4^2 - \frac{3}{4}\delta_1 r_4^3 - g\omega^2 r_2 \cos(\omega\tau) - g\omega^2 r_1 \sin(\omega\tau);\\
U_2 =& k_2 x_0 - k_1 r_1 - \frac{3}{4}\delta_1 r_1^3 + c_1\omega r_2 - \frac{3}{4}\delta_1 r_1 r_2^2 + k_1 r_3 + k_2 r_3 - m_2\omega^2 r_3 + \frac{9}{4}\delta_1 r_1^2 r_3 + \frac{3}{4}\delta_1 r_2^2 r_3 - \frac{9}{4}\delta_1 r_1 r_3^2 + \\
& \frac{3}{4}\delta_1 r_3^3 - c_1\omega r_4 - c_2\omega r_4 + \frac{3}{2}\delta_1 r_1 r_2 r_4 - \frac{3}{2}\delta_1 r_2 r_3 r_4 - \frac{3}{4}\delta_1 r_1 r_4^2 + \frac{3}{4}\delta_1 r_3 r_4^2 + g\omega^2 r_1 \cos(\omega\tau) + g\omega^2 r_2 \sin(\omega\tau);\\
V_2 =& c_2\omega x_0 - c_1\omega r_1 - k_1 r_2 - \frac{3}{4}\delta_1 r_1^2 r_2 - \frac{3}{4}\delta_1 r_2^3 + c_1\omega r_3 + c_2\omega r_3 + \frac{3}{2}\delta_1 r_1 r_2 r_3 - \frac{3}{4} r_2 r_3^2 + k_1 r_4 + k_1 r_4 - m_2\omega^2 r_4 + \\
& \frac{3}{4}\delta_1 r_1^2 + \frac{9}{4}\delta_1 r_2^2 r_4 - \frac{3}{2}\delta_1 r_1 r_3 r_4 + \frac{3}{4}\delta_1 r_3^2 r_4 - \frac{9}{4}\delta_1 r_1 r_2 r_4^2 + g\omega^2 r_2 \cos(\omega\tau) + \frac{3}{4}\delta_1 r_4^3 - g\omega^2 r_1 \sin(\omega\tau).
\end{aligned}
$$

APPENDIX B

Table 3. Physical parameters of the system.

Ω (Hz)	g_{op} (kg)	τ_{op} (s)	$Q_{1(g=0)}$ (ms^{-2})	$Q_{2(g=0)}$ (ms^{-2})	$Q_{1(g=g_{op}),\tau=\tau_{op}}$ (ms^{-2})	$Q_{2(g=g_{op}),\tau=\tau_{op}}$ (ms^{-2})
5	0.070	0.094	5.62	4.88	5.42	4.87
5.5	0.120	0.082	8.08	6.79	7.57	6.75
6	0.081	0.071	11.85	9.60	11.13	9.53
6.5	-0.060	0.128	17.86	13.92	17.16	13.79
7	-0.082	0.111	27.40	20.54	26.19	20.08
7.5	-0.040	0.094	39.39	28.45	38.98	27.91
8	0.071	0.142	44.77	30.86	44.96	29.51
8.5	0.050	0.127	41.01	26.46	42.21	25.57
9	-0.061	0.060	36.17	21.58	38.57	20.64
9.5	-0.090	0.055	32.99	18.04	37.63	16.67
10	-0.110	0.051	31.33	15.54	38.57	13.80
10.5	0.121	0.047	30.84	13.70	41.07	11.64
11	-0.140	0.045	31.31	12.27	46.19	9.52
11.5	-0.150	0.042	32.67	11.07	53.08	7.70
12	-0.151	0.040	34.96	10.00	60.18	6.13
12.5	-0.120	0.039	38.27	9.00	62.40	5.54
13	-0.101	0.037	42.77	8.03	67.45	4.70
13.5	-0.072	0.035	48.61	7.09	70.36	4.28
14	-0.070	0.034	55.85	6.27	80.29	3.66
14.5	-0.039	0.099	64.44	5.79	82.16	2.95
15	0.025	0.062	74.23	5.97	88.10	3.72
15.5	0.018	0.058	84.93	7.04	97.74	4.18
16	-0.010	0.145	96.11	9.01	105.92	5.19
16.5	0.011	0.040	106.65	11.94	114.95	7.13
17	0.060	0.030	30.44	14.54	90.06	7.25
17.5	0.034	0.230	23.38	13.79	16.79	13.17
18	0.030	0.230	19.16	13.29	15.31	12.81